Physica B: Condensed Matter 544 (2018) 23–27

Contents lists available at ScienceDirect

Physica B: Condensed Matter

journal homepage: www.elsevier.com/locate/physb

Current-voltage characteristics of neutron irradiated nanocrystalline silicon carbide (3C—SiC)

Elchin M. Huseynov*

Institute of Radiation Problems of Azerbaijan National Academy of Sciences, AZ 1143, B.Vahabzade 9, Baku, Azerbaijan
Department of Nanotechnology and Radiation Material Science, National Nuclear Research Center, AZ 1073, Inshaatchilar pr. 4, Baku, Azerbaijan

ARTICLE INFO

Keywords:
Nanocrystalline 3C—SiC
Neutron irradiation
I—V characteristics

ABSTRACT

At the present work, nanocrystalline silicon carbide (3C—SiC) irradiated by neutrons (2×10^{13} n/cm^{2}s) up to 20 h. The current–voltage (I—V) characteristics of the nanocrystalline 3C—SiC particles have been investigated in the voltage range of − 100 V to + 100 V with a 5 V step. The slope of the line changed at the I—V characteristic of the nanomaterial after neutron irradiation. Simultaneously, the resistance of nanocrystalline 3C—SiC decreased approximately from 4 MΩ to 1 MΩ after neutron irradiation. Moreover, the Fowler-Nordheim plots showed that the processes occurred in the nanomaterial were directly based on a tunnel effect and no field emission was observed. It is clear from Fowler-Nordheim plots that, thermal activity is dominated at the all experimental intervals.

1. Introduction

Over the past decade, silicon carbide and its various composites have been widely studied by the researchers in the world [1–14]. SiC with attractive physical and chemical resistance has a wide range of applications in extrinsic environments [15–19]. The change of the bandwidth in the 2.2 eV–3.2 eV ranges has led to a wide use of SiC as a semiconductor in electronic systems [20–27]. In the general approach, SiC is a covalently bonded semiconductor. In terms of structure, each Si atom is covalently bonded to four carbon atoms and vice versa. Si and C atoms in SiC have combined in different modifications and have led to the formation of more than 200 polytypes. The most common of these are cubic (3C—SiC) and hexagonal (4H—SiC and 6H—SiC) polytypes. In this study, nanocrystalline 3C—SiC were used, in which the bandgaps was 2.2 eV at room temperature.

Neutron transmutation is one of the most effective methods for the making of doping elements in the nanomaterials. Several effects of neutron irradiation on the 3C—SiC nanocrystals have been investigated at the various scientific studies [28–35]. It is easy to place the doping elements in the atomic lattice of the nanomaterial with the neutron flux. It is clear, newly occurred doping elements will cause the change in the physical properties of the nanomaterial. One of the most common methods for studying physical properties and electronic processes is the I—V characteristic [36–40]. In the general approach, the I—V characteristic of silicon carbide has been widely studied at the various scientific papers [38–43]. However, the I—V characteristic of silicon carbide has been studied less in nano dimensions. Furthermore, neutron irradiation effect on the I—V characteristic, current - resistance, voltage - resistance, and Fowler-Nordheim dependencies have almost not been studied. At the present work, the changes in the physical properties of nanocrystalline 3C—SiC as a result of neutron irradiation have been studied by the I—V characteristic. Moreover, the current-resistance, voltage - resistance, Fowler-Nordheim, voltage -power and specific power-current density dependencies were comparatively analyzed before and after neutron irradiation.

2. Experimental

At the present work, research object is silicon carbide nanoparticles, which have the special surface area (SSA) of 120 m^2/g, the particle size of 18 nm and the density of 0.03 g/cm^3 (true density 3.216 g/cm^3) (US Research Nanomaterials, Inc., TX, USA). Samples irradiated by neutron flux (2×10^{13} n/cm^{2}s) in the central channel (channel A1) of the TRIGA Mark II light water pool-type research reactor at full power (250 kVt) in the Reactor Center of Institute Jozef Stefan (IJS) in Ljubljana, Slovenia. It is important to note that, if the reactor is working at full power then neutron flux parameter as followed: 5.107×10^{12} n/cm^{2}s (1 ± 0.0008, E_n < 625eV) for thermal neutrons, 6.502×10^{12} n/cm^{2}s (1 ± 0.0008, E_n ~ 625eV ÷ 0.1 MeV) for epithermal neutrons, 7.585×10^{12} n/cm^{2}s (1 ± 0.0007, E_n > 0.1 MeV) for fast neutrons and finally, the flux is 1.920×10^{13} n/cm^{2}s (1 ± 0.0005) for all neutrons in the central channel [44–51].

* Institute of Radiation Problems of Azerbaijan National Academy of Sciences, AZ 1143, B.Vahabzade 9, Baku, Azerbaijan.
E-mail address: elchin.h@yahoo.com.

https://doi.org/10.1016/j.physb.2018.05.027
Received 8 May 2018; Received in revised form 17 May 2018; Accepted 18 May 2018
Available online 19 May 2018

3C−SiC nanoparticles have been pressed at press machine (3 kN cm^{-2}) with 2.2 mm height and 15 mm diameter. Prepared samples placed in an aluminum container corresponding to the reactor channel at "Thin Films and Surfaces Physics" Laboratory of IJS. Nanocrystalline 3C−SiC were continuously irradiated in the central channel for 1, 5, 10 and 20 h. The activity of the samples increased up to 3GBq after the neutron irradiation [30]. Therefore, all measurements were carried out approximately 500 h after the neutron irradiation. The silver contacts were put on the surface of the samples in a special condition and their quality was checked (Ogussa, Leitsilber 200). Then, the I−V characteristics of the samples were measured in the "Keithley 238 High Current Source Measurement Unit" at the "Photovoltaics and Optoelectronics Laboratory" of University of Ljubljana. All experiments were conducted at room temperature in the voltage range of −100 V to +100 V and by 5 V steps. Hysteresis measurement was performed (voltage from −100 V to 100 V and vice versa). Bottom side was placed onto the copper plate while the top side was contacted with a contact tip. Each sample was measured on three times where the position of the contact tip was changed. The device was managed by the LabView software and the results corresponding to the obtained values were graphically described in the "OriginPro 9.0" program.

3. Results and discussion

The I−V characteristics of the nanocrystalline 3C−SiC were measured voltage range of −100 V ÷ + 100 V at room temperature. The experiments revealed that there were differences in dependence of I−V, P - U, etc. before and after neutron radiation. The I−V characteristic of nanocrystalline 3C−SiC before and after neutron radiation has been described at Fig. 1.

The linear plot at the I−V characteristic and small angle slope corresponding to voltage axis, described relatively high resistance before neutron irradiation. Simultaneously, plot symmetry corresponding to the zero points of voltage and current axis indicates that the samples are sufficiently clean [39]. Moreover, there is a steepness (slope) of the line changed at the I−V characteristic of the nanocrystalline 3C−SiC after neutron irradiation. In this way, after neutron irradiation, the plots angle with the voltage axis sharply increased in the I−V characteristic of the nanocrystalline 3C−SiC. On the other hand, it is known that the cotangent of this angle directly characterizes the resistance of the sample: cotα = R. An increased the angle formed by the plots and the voltage axis after the neutron irradiation causes a decrease the resistance of the sample. Thus, the electrical conductivity of the samples increases after neutron irradiation, which has been proven in other experiments [32,35]. Like previous experiments, this increase can be explained by the neutron transformation, dangling bonds, formation of defects, or charge carriers [28–35]. The shifting curves also become in current - resistance and voltage - resistance plots after neutron irradiation (Fig. 2).

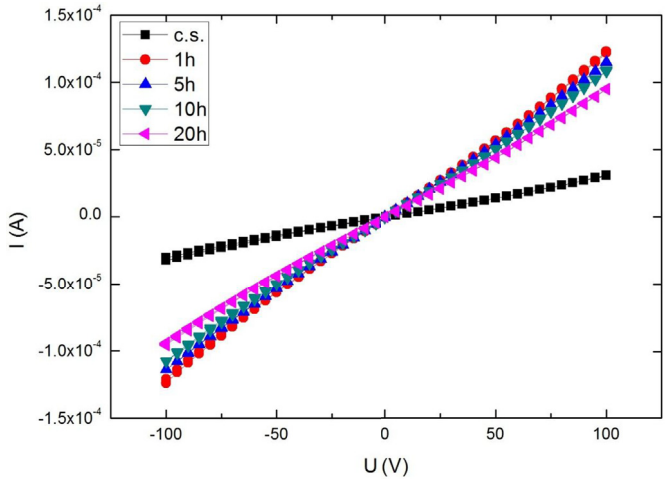

Fig. 1. I–V characteristics of the nanocrystalline 3C−SiC before (c.s.) and after (1 h, 5 h, 10 h, and 20 h) neutron irradiation.

As can be seen from Fig. 2, the resistance of nanocrystalline 3C−SiC is sharply reduced after neutron irradiation. At the same time, in Fig. 2a, a shifting occurs in the current-resistance plots in the direction of resistance with respect to the current axis. It is possible the amount of the current passing through this environment increases after the neutron radiation according to the curve shifts. As can be seen from Fig. 2b, the value of positive and negative voltage almost does not affect the resistance of the sample. However, there is a sharp decrease in resistance of nanocrystalline 3C−SiC after neutron irradiation. It should be noted that the resistance partly decreases before neutron irradiation due to the voltage increasing (Fig. 2b). Simultaneously, the value of the resistance after neutron irradiation does not depend on voltage. The Fowler-Nordheim plots were compared before and after neutron irradiation for the investigated of direct tunneling or field emission of nanocrystalline 3C−SiC (Fig. 3).

Simply, tunnel barrier at the molecular level is characterized by Simmons's approach in the I−V dependencies [52–55]:

$$I = \frac{qA}{4\pi^2\hbar d^2}\left[\left(\varphi - \frac{qV}{2}\right)\exp\left(-\frac{2d\sqrt{2m^*}}{\hbar}\sqrt{\varphi - \frac{qV}{2}}\right) - \left(\varphi + \frac{qV}{2}\right)\exp\left(-\frac{2d\sqrt{2m^*}}{\hbar}\sqrt{\varphi + \frac{qV}{2}}\right)\right] \quad (1)$$

here, A is the junction area, d is the barrier width, m^* is the effective mass of the charge carrier, φ is the barrier height, $\hbar$ is the reduced Planck's constant and q is the electron charge. The tunneling probability of the process depends on the shape of the barrier of the chosen sample in the Fowler-Nordheim plots [55]. In limiting case, if we take a barrier as a rectangular, the I−V dependencies is directly explained by the tunnel effect [52–55]:

$$I \infty V \exp\left(-\frac{2d\sqrt{2m^*\varphi}}{\hbar}\right) \quad (2)$$

On the other hand, if the applied voltage exceeds the barrier height, the barrier turns into a triangular form from a rectangular shape and this triangular deformation causes the formation of the Fowler-Nordheim tunnel (field emission) [52–55]. In this case, I−V dependence can be characterized by the equation below:

$$I \infty V^2 \exp\left(-\frac{4d\sqrt{2m^*\varphi^3}}{3\hbar qV}\right) \quad (3)$$

Fowler-Nordheim plots explain directly whether the process is a tunnel or field emission. In this case, Eqs. (2) and (3) can be expressed as follows [52–55]:

$$\ln\left(\frac{I}{V^2}\right) \infty \ln\left(\frac{1}{V}\right) - \frac{2d\sqrt{2m^*\varphi}}{\hbar} \quad (4)$$

$$\ln\left(\frac{I}{V^2}\right) \infty -\left(\frac{1}{V}\right)\frac{4d\sqrt{2m^*\varphi^3}}{3\hbar q} \quad (5)$$

It should be noted that if Fowler-Nordheim's plots are logarithmic, the process is explained by the direct tunneling and if it is a negative slope line, the process can be explained by field emission [54,55]. Existing ln(A/V^2) vs. 1/V plots in Fig. 3 corresponds to Eq. (2) which is can distinctly show the direct tunneling [52–55]. The Fowler-Nordheim plots in Fig. 3 shows that the process is directly based on the tunnel effect in nanocrystalline 3C−SiC at the temperature at which experiments are carried out, and no field emission is observed. The curves observed in Fig. 3 show that thermal activity before and after neutron irradiation in the nanocrystalline 3C−SiC is dominant at all intervals

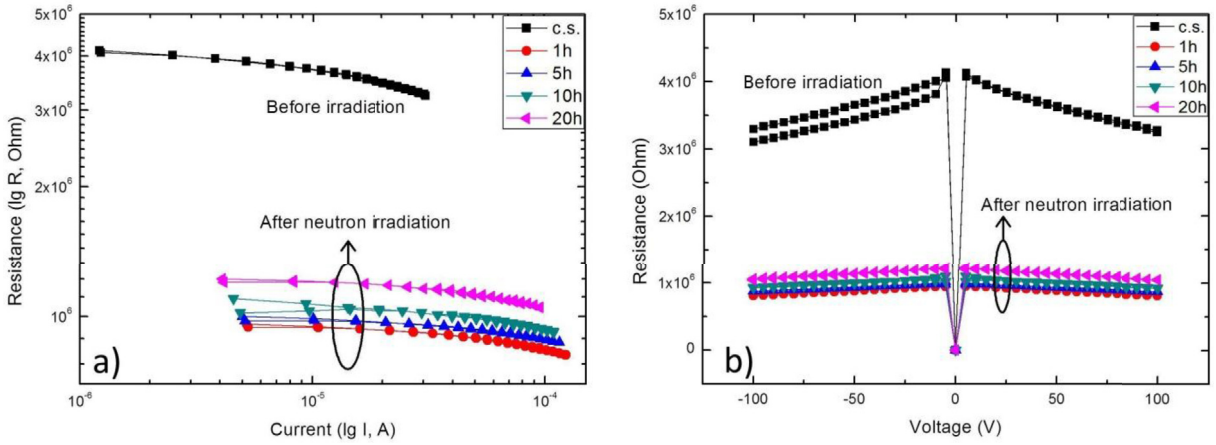

Fig. 2. The current-resistance (a) and voltage - resistance (b) plots of the nanocrystalline 3C−SiC before (c.s.) and after (1 h, 5 h, 10 h, and 20 h) neutron irradiation.

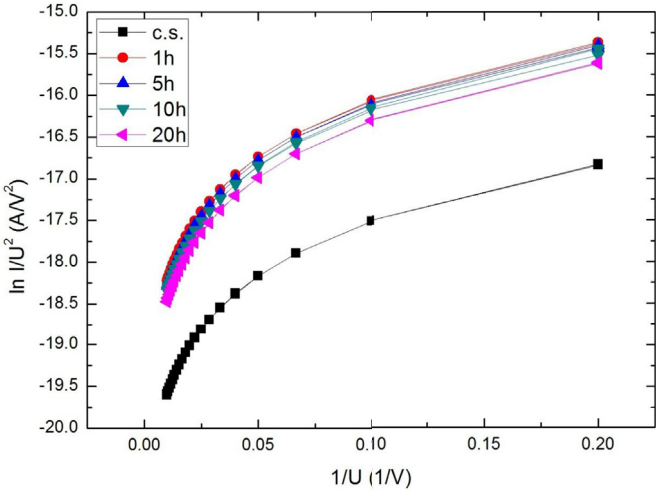

Fig. 3. Fowler-Nordheim plots of nanocrystalline 3C−SiC before (c.s.) and after (1 h, 5 h, 10 h, and 20 h) neutron radiation.

[55].

Voltage - Power characteristics were examined to determine the effective operating voltage in the nanocrystalline 3C−SiC (Fig. 4).

Voltage - power characteristics show that more power change is observed in the voltage change after neutron radiation. However, the Voltage-Power plots of the nanocrystalline 3C−SiC are not observed with any peaks in the shown voltage range, in contrast to the photo-transistors used in solar panels. This means that the effective operating voltage is more than the 100 V voltage in this nanomaterial. The effect of neutron radiation is obviously observed from the plots of specific power vs. current density (Fig. 5).

The slope isn't observed in specific power vs. current density plots as a result of neutron radiation. However, it is clear from Fig. 5, after neutron irradiation plots, shifted. Observed shifting in the specific power vs. current density plots after neutron irradiation can be explained by the neutron transformation, dangling bonds, the formation of defects or additional charge carriers similar to the other cases.

Generally, the changes observed in I−V characteristic after neutron irradiation are closely linked to neutron transmutation elements. The ^{30}Si turns into the ^{31}Si isotope by capture one neutron in the nanocrystalline 3C−SiC as a result of neutron irradiation. As ^{31}Si isotope is β active isotope, it turns to ^{31}P isotope as a result of nuclear transformation ($^{30}Si(n,\gamma)^{31}Si \rightarrow {}^{31}P + \beta^{-}(T_{1/2} = 2.6h)$). ^{31}P isotope behaves like n-type doping elements in the nanocrystalline 3C−SiC. Thus, an increase in the concentration of the ^{31}P isotopes after neutron irradiation is manifested directly in the I−V characteristic.

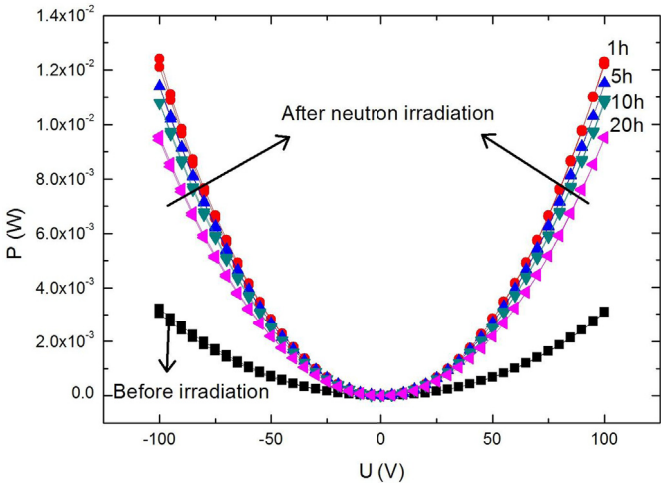

Fig. 4. Voltage-power plots of nanocrystalline 3C−SiC before (c.s.) and after (1 h, 5 h, 10 h and 20 h) neutron irradiation.

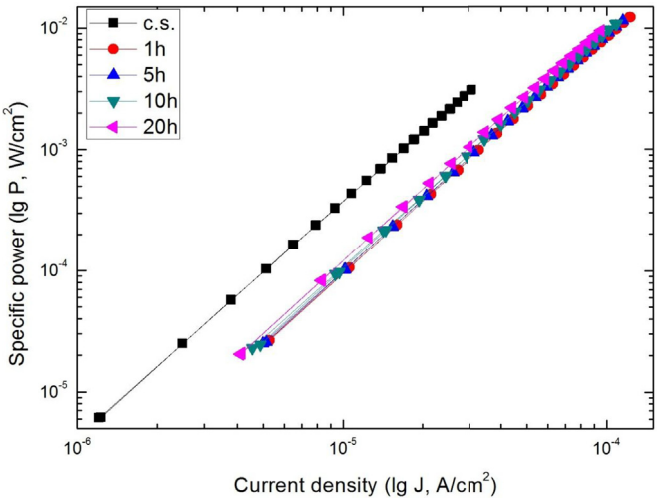

Fig. 5. Specific power-current density dependencies of nanocrystalline 3C−SiC before (c.s.) and after (1 h, 5 h, 10 h, and 20 h) neutron radiation.

4. Conclusions

The slope of plots was observed in the I–V characteristic of the nanocrystalline 3C–SiC after neutron irradiation. An increase slope of plots corresponding to voltage axis after the neutron irradiation is an indication of the decrease of resistance of the sample. The slope of plots revealed that the resistance of the nanocrystalline 3C–SiC decreasing from approximately 4 MΩ–1 MΩ after neutron irradiation. The reason for this decline is associated with the neutron transmutation elements, dangling bonds, the existence of defects, or additional charge carriers. Simultaneously, Fowler-Nordheim plots have shown that there is a direct tunnel junction in nanocrystalline 3C–SiC. There is no field emission in nanocrystalline 3C–SiC at the experimental temperatures and the process is directly based on the tunnel effect. Moreover, Fowler-Nordheim plots disclosed that thermal activity in the nanocrystalline 3C–SiC is dominant at all intervals before and after neutron irradiation.

Acknowledgments

This work was supported by the Science Development Foundation under the President of the Republic of Azerbaijan – Grant № EİF/GAM-4-BGM-GİN-2017-3(29)-19/01/1. I gratefully acknowledge the assistance of my colleagues from the Institute of Radiation Problems of the Azerbaijan National Academy of Sciences, the National Nuclear Research Center (NNRC) and the Reactor Infrastructure Center (RIC)" at the Institute Jožef Stefan (IJS) and Faculty of Electrical Engineering “Laboratory of Photovoltaics and Optoelectronics” at the University of Ljubljana, Slovenia. I would like to thank Prof. Dr. Luka Snoj and Anže Jazbec for providing irradiated samples in TRIGA Mark II type research reactor and Prof. Dr. Marko Topič and Marko Jošt for encouraging discussions.

References

[1] Yu Zhou, Junfeng Wang, Xiaoming Zhang, Ke Li, Jianming Cai, Weibo Gao, Self-protected thermometry with infrared photons and defect spins in silicon carbide, Phys. Rev. Appl. 8 (2017) 044015.
[2] M. Sedighi, V.B. Svetovoy, G. Palasantzas, Casimir force measurements from silicon carbide surfaces, Phys. Rev. B 93 (2016) 085434.
[3] Andrey A. Stepashkin, Dilyus I. Chukov, Sergey D. Kaloshkin, et al., Carbonized elastomer based composites filled with carbon fillers and silicon carbide, Mater. Lett. 215 (2018) 288–291.
[4] Greg Calusine, Alberto Politi, David D. Awschalom, Cavity-enhanced measurements of defect spins in silicon carbide, Phys. Rev. Appl. 6 (2016) 014019.
[5] Najmeh Delavari, Mahmoud Jafari, Electronic and optical properties of hydrogenated silicon carbide nanosheets: a DFT study, Solid State Commun. 275 (2018) 1–7.
[6] Kierstin Daviau, Kanani K.M. Lee, Decomposition of silicon carbide at high pressures and temperatures, Phys. Rev. B 96 (2017) 174102.
[7] Abram L. Falk, Paul V. Klimov, Viktor Ivády, Krisztián Szász, David J. Christle, William F. Koehl, Ádám Gali, David D. Awschalom, Optical polarization of nuclear spins in silicon carbide, Phys. Rev. Lett. 114 (2015) 247603.
[8] Hsun-Chi Li, Wei-Sheng Chen, Recovery of silicon carbide from waste silicon slurry by using flotation, Energy Procedia 136 (2017) 53–59.
[9] Sara Toth, Peter Nemeth, Peter Racz, et al., Silicon carbide nanocrystals produced by femtosecond laser pulses, Diam. Relat. Mater. 81 (2018) 96–102.
[10] Bo Peng, Yuming Zhang, Yutian Wang, Hui Guo, Lei Yuan, Renxu Jia, Ferromagnetism observed in silicon-carbide-derived carbon, Phys. Rev. B 97 (2018) 054401.
[11] I. Vivaldo, M. Moreno, A. Torres, et al., A comparative study of amorphous silicon carbide and silicon rich oxide for light emission applications, J. Lumin. 190 (2017) 215–220.
[12] Roland Nagy, Matthias Widmann, Matthias Niethammer, Durga B. R. Dasari, Ilja Gerhardt, Öney O. Soykal, Marina Radulaski, Takeshi Ohshima, Jelena Vučković, Nguyen Tien Son, Ivan G. Ivanov, Sophia E. Economou, Cristian Bonato, Sang-Yun Lee, Jörg Wrachtrup, Quantum properties of dichroic silicon vacancies in silicon carbide, Phys. Rev. Appl. 9 (2018) 034022.
[13] K. Kefif, Y. Bouizem, A. Belfedal, J.D. Sib, D. Benlakehal, L. Chahed, Hydrogen related crystallization in silicon carbide thin films, Optik - Int. J. Light Electron Optic. 154 (2018) 459–466.
[14] Junfeng Wang, Yu Zhou, Xiaoming Zhang, Fucai Liu, Yan Li, Ke Li, Zheng Liu, Guanzhong Wang, Weibo Gao, Efficient generation of an array of single silicon-vacancy defects in silicon carbide, Phys. Rev. Appl. 7 (2017) 064021.
[15] L.L. Snead, T. Nozawa, M. Ferraris, et al., Silicon carbide composites as fusion power reactor structural materials, J. Nucl. Mater. 417 (1–3) (2011) 330–339.
[16] P.Z. Takacz, T.L. Hursman, J.T. Williams, Application of silicon carbide to synchrotron radiation mirrors, Nucl. Instrum. Meth. Phys. Res. 222 (1–2) (1984) 133–145.
[17] Robert W. Flammang, John G. Seidel, Frank H. Ruddy, Fast neutron detection with silicon carbide semiconductor radiation detectors, Nucl. Instrum. Methods Phys. Res. Sect. A Accel. Spectrom. Detect. Assoc. Equip. 579 (1) (2007) 177–179.
[18] T. Nozawa, T. Hinoki, A. Hasegawa, et al., Recent advances and issues in development of silicon carbide composites for fusion applications, J. Nucl. Mater. 386–388 (2009) 622–627.
[19] Yutai Katoh, Lance L. Snead, Izabela Szlufarska, William J. Weber, Radiation effects in SiC for nuclear structural applications, Curr. Opin. Solid State Mater. Sci. 16 (3) (2012) 143–152.
[20] M. Perani, D. Cavalcoli, M. Canino, et al., Electrical properties of silicon carbide/silicon rich carbide multilayers for photovoltaic applications, Sol. Energy Mater. Sol. Cell. 135 (2015) 29–34.
[21] José Sánchez-González, Angel L. Ortiz, Fernando Guiberteau, Carmen Pascual, Complex impedance spectroscopy study of a liquid-phase-sintered α-SiC ceramic, J. Eur. Ceram. Soc. 27 (13–15) (2007) 3935–3939.
[22] Hui Deng, Nian Liu, Katsuyoshi Endo, Kazuya Yamamura, Atomic-scale finishing of carbon face of single crystal SiC by combination of thermal oxidation pretreatment and slurry polishing, Appl. Surf. Sci. 434 (2018) 40–48.
[23] I. Vivaldo, M. Moreno, A. Torres, et al., A comparative study of amorphous silicon carbide and silicon rich oxide for light emission applications, J. Lumin. 190 (2017) 215–220.
[24] Gabriela Huminic, Angel Huminic, Claudiu Fleaca, Florian Dumitrache, Ion Morjan, Thermo-physical properties of water based SiC nanofluids for heat transfer applications, Int. Commun. Heat Mass Tran. 84 (2017) 94–101.
[25] Kai Wei, Kaiyu Wang, Xiangmeng Cheng, et al., Structural and thermal analysis of integrated thermal protection systems with C/SiC composite cellular core sandwich panels, Appl. Therm. Eng. 131 (2018) 209–220.
[26] Bejoy N. Pushpakaran, Anitha Sarah Subburaj, Stephen B. Bayne, John Mookken, Impact of silicon carbide semiconductor technology in photovoltaic energy system, Renew. Sustain. Energy Rev. 55 (2016) 971–989.
[27] Peipei Wang, Hejun Li, Jia Sun, Ruimei Yuan, Longxin Zhang, Yulei Zhang, Tao Li, The effect of HfB2 content on the oxidation and thermal shock resistance of SiC coating, Surf. Coating. Technol. 339 (2018) 124–131.
[28] Elchin M. Huseynov, Neutron irradiation, amorphous transformation and agglomeration effects on the permittivity of nanocrystalline silicon carbide (3C-SiC), Nano 13 (3) (2018) 1830002.
[29] Elchin M. Huseynov, Electrical impedance spectroscopy of neutron-irradiated nanocrystalline silicon carbide (3C-SiC), Appl. Phys. A 124 (2018) 19.
[30] Elchin Huseynov, Anze Jazbec, Trace elements study of high purity nanocrystalline silicon carbide (3C-SiC) using k0-INAA method, Phys. B Condens. Matter 517 (2017) 30–34.
[31] Elchin M. Huseynov, Permittivity-frequency dependencies study of neutron-irradiated nanocrystalline silicon carbide (3C-SiC), Nano 12 (6) (2017) 1750068.
[32] Elchin M. Huseynov, Neutron irradiation effects on the temperature dependencies of electrical conductivity of silicon carbide (3C-SiC) nanoparticles, Silicon 10 (3) (2018) 995–1001.
[33] Elchin M. Huseynov, Investigation of the agglomeration and amorphous transformation effects of neutron irradiation on the nanocrystalline silicon carbide (3C-SiC) using TEM and SEM methods, Phys. B Condens. Matter 510 (2017) 99–103.
[34] Elchin Huseynov, Adil Garibov, Effects of neutron flux on the temperature dependencies of permittivity of 3C-SiC nanoparticles, Silicon 9 (5) (2017) 753–759.
[35] Elchin Huseynov, Neutron irradiation and frequency effects on the electrical conductivity of nanocrystalline silicon carbide (3C-SiC), Phys. Lett. A 380 (38) (2016) 3086–3091.
[36] Akimori Tabata, Yoshikazu Imori, Current density–voltage and admittance characteristics of hydrogenated nanocrystalline cubic SiC/crystalline Si heterojunction diodes prepared with varying H2 gas flow rates, Solid State Electron. 104 (2015) 33–38.
[37] R.D.Y. Hills, A. Kusmartseva, F.V. Kusmartsev, Current-voltage characteristics of Weyl semimetal semiconducting devices, Veselago lenses, and hyperbolic Dirac phase, Phys. Rev. B 95 (2017) 214103.
[38] M.L. Megherbi, F. Pezzimenti, L. Dehimi, et al., Analysis of different forward current–voltage behaviours of Al implanted 4H-SiC vertical p–i–n diodes, Solid State Electron. 109 (2015) 12–16.
[39] R. Tiskumara, R.P. Joshi, D. Mauch, J.C. Dickens, A.A. Neuber, Analysis of high field effects on the steady-state current-voltage response of semi-insulating 4H-SiC for photoconductive switch applications, J. Appl. Phys. 118 (2015) 095701.
[40] Chr Schröder, W. Heiland, R. Held, W. Loose, Analysis of reverse current–voltage characteristics of Ti/6H–SiC Schottky diodes, Appl. Phys. Lett. 68 (1957) 1996.
[41] D.B. Dimitrov, Current-voltage characteristics of porous-silicon layers, Phys. Rev. B 51 (1995) 1562.
[42] Atsushi Nishikawa, Kazuhide Kumakura, Tetsuya Akasaka, Toshiki Makimoto, Current-voltage characteristics of p - In Ga N / n - Ga N vertical conducting diodes on n + - Si C substrates, Appl. Phys. Lett. 87 (2005) 233505.
[43] H.S. Kong, J.W. Palmour, J.T. Glass, R.F. Davis, Temperature dependence of the current-voltage characteristics of metal-semiconductor field-effect transistors in n-type β-SiC grown via chemical vapor deposition, Appl. Phys. Lett. 51 (1987) 442.
[44] Tanja Goričanec, Gašper Žerovnik, Loïc Barbot, Damien Fourmentel, Christophe Destouches, Anže Jazbec, Luka Snoj, Evaluation of neutron flux and fission rate distributions inside the JSI TRIGA Mark II reactor using multiple in-core fission chambers, Ann. Nucl. Energy 111 (2018) 407–440.
[45] Luka Snoj, Gasper Zerovnik, Andrej Trkov, Computational analysis of irradiation facilities at the JSI TRIGA reactor, Appl. Radiat. Isot. 70 (2012) 483–488.

[46] K. Ambrožič, G. Žerovnik, L. Snoj, Computational analysis of the dose rates at JSI TRIGA reactor irradiation facilities, Appl. Radiat. Isot. 130 (2017) 140–152.
[47] P. Filliatre, C. Jammes, L. Barbot, D. Fourmentel, B. Geslot, I. Lengar, A. Jazbec, L. Snoj, G. Žerovnik, Experimental assessment of the kinetic parameters of the JSI TRIGA reactor, Ann. Nucl. Energy 83 (2015) 236–245.
[48] G. Zerovnik, et al., Validation of the neutron and gamma fields in the JSI TRIGA reactor using in-core fission and ionization chambers, Appl. Radiat. Isot. 96 (2015) 27–35.
[49] R. Henry, I. Tiselj, L. Snoj, Analysis of JSI TRIGA MARK II reactor physical parameters calculated with TRIPOLI and MCNP, Appl. Radiat. Isot. 97 (2015) 140–148.
[50] Tanja Kaiba, Gasper Zerovnik, Anze Jazbec, Ziga Stancar, Loic Barbot, Damien Fourmentel, Luka Snoj, Validation of neutron flux redistribution factors in JSI TRIGA reactor due to control rod movements, Appl. Radiat. Isot. 104 (2015) 34–42.
[51] A. Kolsek, V. Radulovic, A. Trkov, L. Snoj, Using TRIGA Mark II research reactor for irradiation with thermal neutrons, Nucl. Eng. Des. 283 (2015) 155–161.
[52] G. Pananakakis, G. Ghibaudo, R. Kies, C. Papadas, Temperature dependence of the Fowler–Nordheim current in metaloxide degenerate semiconductor structures, J. Appl. Phys. 78 (1995) 2635.
[53] Jeremy M. Beebe, BongSoo Kim, J.W. Gadzuk, C. Daniel Frisbie, James G. Kushmerick, Transition from direct tunneling to field emission in metal-molecule-metal junctions, Phys. Rev. Lett. 97 (2006) 026801.
[54] Seong Ho Choi, BongSoo Kim, C. Daniel Frisbie, Electrical resistance of long conjugated molecular wires, Science 320 (5882) (2008) 1482–1486.
[55] Evan S.H. Kang, Eunseong Kim, Multi-barrier field-emission behavior in PBTTT thin films at low temperatures, Sci. Rep. 5 (2015) 8396.